A Brief Exploration of Astrophysical Applications for Terahertz Spectroscopy

A Major Qualifying Project Submitted to the
Faculty of Worcester Polytechnic Institute in
partial fulfillment of the requirements for the
Degree in Bachelor of Science In Physics

By:
Valerie Courtemanche
Jackson Morse
Zetta C. Rajaniemi
Date:
May 06, 2021

Project Advisors:
Professor Douglas Petkie, WPI
Professor Rudra Kafle, WPI

This report represents the work of WPI undergraduate students submitted to the faculty as evidence of a degree requirement. WPI routinely publishes these reports on its website without editorial or peer review. For more information about the projects program at WPI, see http://www.wpi.edu/Academics/Projects

Abstract

Terahertz spectroscopy is a relatively new technology in the field of observational astrophysics. This project began by learning the uses and history of this field before applying data processing methods to data collected by the Atacama Large Millimeter/Submillimeter Array (ALMA) telescope. Three studies that looked at different astronomical objects/phenomena were chosen for analysis. Data was taken from the ALMA project archive and analyzed using the Cube Analysis and Rendering Tool for Astronomy (CARTA). One study looked at stellar formation in a high red-shifted galaxy and showed detections of doubly-ionized oxygen (O III). Another looked at the dust production of supernovae to determine if supernovae are significant producers of dust. The last study looked at the potential detection of phosphine within the atmosphere of Venus. Methodologies were carefully recorded and further research questions were presented upon project conclusion.

Acknowledgments

We would like to thank our advisors for their help and guidance on this project as well as our friends and family for supporting us throughout our academic careers.

Zetta would specifically like to thank her parents, roommates, boyfriend, and the Dunkin workers for motivating her through this project.

Contents

Table of Figures

Table of Tables

Chapter 1: Introduction

Since Galileo pointed the first telescope toward the moons of Jupiter, humans have been trying to develop better technology for looking at the heavens. We began by magnifying distant objects using optics and eventually found ways to see light outside of the visible range. Today, scientists can look to the very edge of the universe using almost any wavelength of light they would like. One of the newest developments on this front is terahertz spectroscopy, which looks at light in the range of 0.1-20 THz (Beard, 2002).

Terahertz spectroscopy is a somewhat new branch of technology that has helped make great strides in the field of observational astrophysics (Kulesa, 2011). It can be used to analyze the atomic and molecular abundances in the atmospheres of nearby planets or even comets to discern their contents and potentially identify signs of extraterrestrial life. It can help us learn about the interstellar medium and how it has evolved over time, giving us a peek into the entire life cycle how stars form and die. It can even help us learn about how stars and galaxies formed in the early universe just after the Big Bang. Each of these ideas will be explored in the results section of this paper.

One of the most well-known observatories looking at the cosmos in the terahertz range is the Atacama Large Millimeter/Submillimeter Array (ALMA) in Chile.

Figure 1.1 A picture of ALMA, seen from the Chilean desert site.
Credit: https://public.nrao.edu/telescopes/alma/

Development began on ALMA in 2004 and the first observations were made in late 2011 (ALMA, n.d.). Since then, astronomers have been pointing the radio telescope all over the universe from our own solar system to distant galaxies. One main advantage terahertz

spectroscopy, and radio observation in general, provides is the ability to detect wavelengths that are much longer than any wavelengths in the optical range (Strobel, 2019). Radio arrays, like ALMA's, are massive compared to their optical counterparts. Even top tier optical telescopes, such as the ones from Keck Observatory on Mauna Kea, are 10-meter diameter telescopes, compared to ALMA's array of 54 12-meter diameter (plus 12 7-meter diameter) radio dishes that act as a singular telescope (DeVorkin, 2010), (ALMA, n.d.). Other radio dishes from the Very Large Array telescope are 25-meters in diameter each, quite the difference from the seemingly tiny optical telescopes (Strobel, 2019).

So, why is the size of the dish important here? It becomes important for when astronomers decide to observe stellar objects further away than the reach of optical wavelengths. Because the radio wavelengths are much longer than optical wavelengths, this means they have less energy, and thus need a much larger dish or array to acquire information about a certain stellar object (Strobel, 2019). These observations have led to a variety of data processing techniques and platforms. The purpose of this project was to learn how to operate one of these platforms and extract useful information from it.

While a variety of data processing platforms were considered, it was eventually decided that the Cube Analysis and Rendering Tool for Astronomy (CARTA) would be used as it was the most accessible for all team members (ALMA Archive, n.d.). Each team member then chose a different published study to analyze and learn from. One study looked at stellar formation in a high redshift galaxy and showed findings of O III emission lines. Another looked at the dust production of supernovae to determine if supernovae were significant producers of dust. The last study looked at the potential detection of phosphine within the atmosphere of Venus. The methodology used in each study was carefully analyzed and some of the findings from each one were recreated. The ultimate goal of this endeavor was to learn the data processing techniques used by professional astronomers and astrophysicists while identifying future research questions.

Chapter 2: Background

The purpose of this chapter is to provide a brief overview of terahertz spectroscopy and what is needed to use it for observational astrophysical research. It begins with an explanation of how spectroscopic data is produced and interpreted as well as what specifically defines terahertz spectroscopy. The middle section of this chapter presents the technology used in collecting data from astronomical sources with a strong focus on the Atacama Large Millimeter/Submillimeter Array (ALMA). We then conclude with an overview of data processing platforms that can be used to analyze data collected by ALMA with special attention paid to the Cube Analysis and Rendering Tool for Astronomy (CARTA). This is meant to provide the reader with a working understanding of the concepts and tools utilized for the completion of this project.
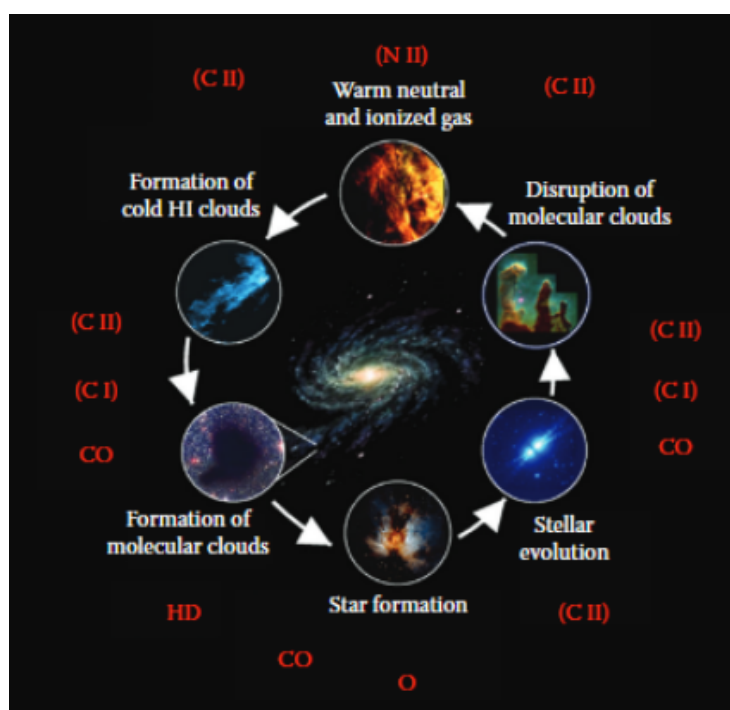
Figure 2.1 Life cycle of the Interstellar Medium. Credit: *Terahertz Astronomy* by Christopher K. Walker

Shown in Figure 2.1 above is the lifecycle of the interstellar medium (ISM) (Walker, 2015). Each of the topics studied in this project represent a different stage of this cycle. The first topic looked at star formation in deep space, specifically at O III emission. The second topic focused on the area between stellar evolution and disruption of molecular clouds (after a

supernova explosion) at carbon emission. The third topic looked at a planetary application of terahertz spectroscopy between star formation and stellar evolution, looking at phosphine emission.

Section 2.1 - A Brief Introduction to Terahertz Spectroscopy

Spectroscopy is the science of using light to find out what elements and molecular compounds things are made of by studying their spectra. It takes advantage of how the photons that make up light interact with atoms and molecules, which are able to change the way we perceive light by absorbing and emitting photons. To understand this process, we'll start by looking at a singular atom using the Bohr model of a hydrogen atom and continue to describe vibrational and rotational spectroscopy of molecules in the Terahertz region.

2.1.1 - How Atoms Affect Light

Hydrogen has a single electron that orbits its nucleus on levels referred to as orbitals and each orbital has a different radius that corresponds to a unique energy level (Clark, 2000). The orbital with the smallest radius has the lowest energy and as the orbital radius increases, so does the energy. For simplicity, let's look at the two lowest energy levels, E_1 and E_2 (Figure 2.2). The difference between these energy levels is represented by $\Delta E = E_2 - E_1$ (Ryden, 2010, 119).
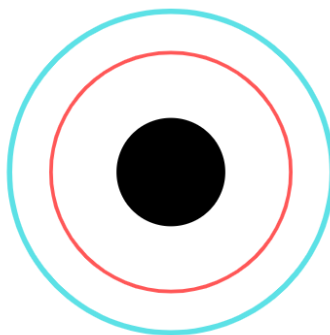
Figure 2.2 A model of the Hydrogen atom. The red line represents
the lowest orbital of energy E_1 and the blue line represents the second
orbital of energy E_2.

The differences between the energy levels of orbitals are what allows for light to interact with the electrons inside of atoms through a process known as photoexcitation. The process can be split into three phases, as shown below in Figure 2.3.

Phase 1   Phase 2   Phase 3
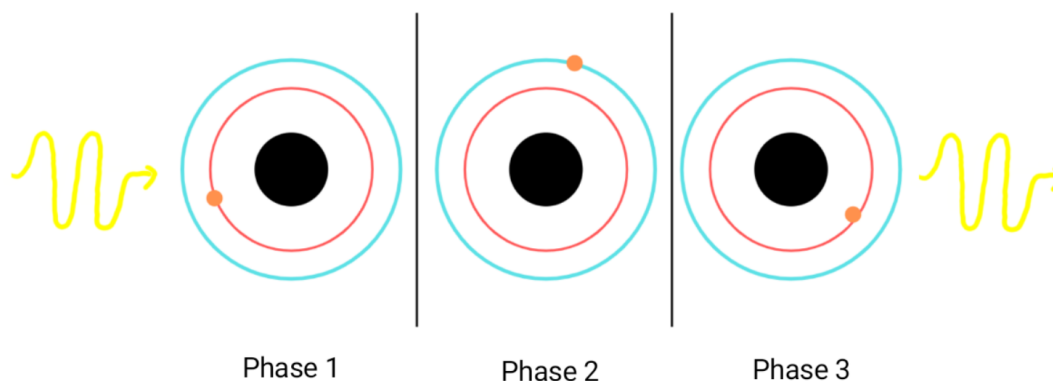
Figure 2.3 A diagram of a photon interacting with a hydrogen atom. The red line
represents the lowest orbital of energy E_1. The blue line represents the second orbital of
energy E_2. The beige circle is an electron. The yellow lines are photons. The three phases
are described in detail below

In Phase 1, a photon, referred to as the incident photon, in this case, hits the atom (Young, 2020, p. 1300). If the incident photon has an energy equal to ΔE, it can be absorbed by the atom. (Ryden, 2010, p. 118). This brings us to Phase 2 where the electron is able to take the energy from the incident photon and jump from its ground position on the E_1 orbital to an excited state on the E_2 orbital (Ryden, 2021, p.118). This is an unstable state and the electron will eventually fall back to its ground position. That will bring us to Phase 3. When the electron falls back to the

lower energy state the atom gets excess energy that it has to expel. This energy is expelled in the form of an emitted photon which has an energy equal to ΔE (Ryden, 2020, p. 118).

This same basic principle applies to any atom, regardless of the number of electrons and orbitals. If the incident photon has a high enough energy, the electron can even jump multiple orbitals. The atom can then emit one photon or several photons, but the energy of the emitted photon(s) will always be equal to that of the incident photon (Ryden, 2010, p. 121). These defined energy levels mean that different atoms can absorb or emit photons of different energies, a principle which also applies to molecules.

2.1.2 - How Molecules Interact With Light

Another layer of complexity is added when we begin to consider entire molecules instead of a singular atom. The same idea of only photons with specific energy levels being able to interact with molecules applies, but instead of a singular electron moving the entire molecule reacts to the light. Molecules have specific, quantized energy levels the same way orbitals do, only this time the energy is the vibrational or rotational energy of the molecule.

Vibrational energy is concerned with the bonds between the atoms that make up the molecules. These bonds can change either through stretching or bending. Stretching refers to when the distance between atoms in a molecule becomes longer or shorter and bending refers to when the angle between those bonds changes (Figure 2.4) (Cameron, 2020). Both of these vibration types occur with specific amounts of energy when the molecule absorbs or emits a photon of light. This allows molecules to make the same kind of visual changes to light that atoms do. Because the energy needed for each type of vibration is specific and unique to each molecule, each molecule will affect light in a different way (Siesler, 2015).
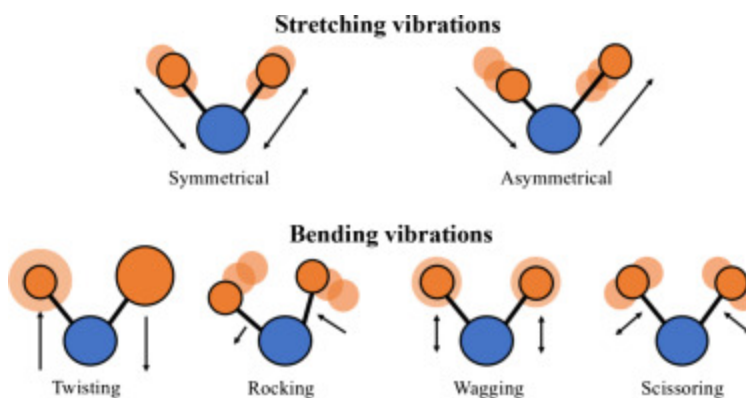
Figure 2.4 A diagram depicting different types of molecular vibrations.
Credit: https://www.sciencedirect.com/science/article/pii/B9780128186107000104

Rotational energy is a bit more what it sounds like. A rotating molecule can genuinely be analogized to a spinning top. When looking at how much energy is in the top we look at its angular velocity (ω) and its moment of inertia (I) (Nave, n.d.). The angular velocity refers to the rate at which the top can complete one spin. The moment of inertia is a product of the top's mass and radius and it determines how hard it is to make the top spin. By combining these two values, you can find the rotational energy of the top. A similar process is undergone when looking at a rotating molecule, but in this case, we need to introduce a little quantum mechanics.

Molecules can rotate only at very specific energies, like how atoms have orbitals of specific energy levels. Because these energies are so specific and fixed they are said to be quantized which means we need to change our language a little bit. When looking at very small things like molecules, the idea of rotational energy described above, now referred to as spin, becomes only half of the concept. The other half can be pictured when the top starts to fall and begins to wobble. The top of the top will start rotating around the axis at the center of its motion. Molecules can have a similar wobble, now called a precession. By combining the spin and precession, known as J and K quantum numbers respectively, we can find the rotational energy of a molecule (Rotational Spectroscopy of Diatomic Molecules, 2020).
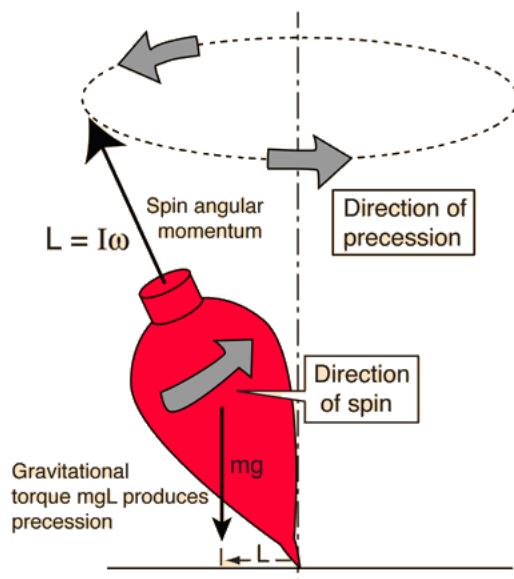
Figure 2.5 A diagram of how a spinning top moves for reference.
Credit: http://hyperphysics.phy-astr.gsu.edu/hbase/top.html

Molecules with rotational energy interacting with light are a little more complicated than atoms interacting with light. When an atom interacts with light, only one thing can change - which electron the orbital is on. In this case, the spin and/or precession can change whenever a molecule absorbs or emits a photon. This change is referred to as a rotational transition and scientists need a way to show what change occurred where. In writing, when defining a rotational transition, it is written as $J_iK_i{\rightarrow}J_fK_f$ where J_iK_i are the initial values for spin and precession while J_fK_f are the final values (Rotational Spectroscopy of Diatomic Molecules, 2020). Due to the quantized nature of rotational energy states, this notation is often written as integers with 0 representing the lowest energy level, 1 being one energy level higher, and so on so that a transition from the lowest energy state on in spin may be written as $00{\rightarrow}10$ (Houghton, 2020).

2.1.3 - How Spectroscopy Works

The way that atoms and molecules interact with light allows scientists to analyze something (mainly gases) and know what they are composed of based on the idea of spectra. The entire electromagnetic spectrum includes light corresponding to photons of every energy level

(NASA, 2013). Scientists can take a portion of this light and see how atoms and molecules interact with it to help determine what they are looking at. This is done using the principle that a beam of light filtered through a prism will be broken down into a distributed spectrum (Figure 2.6) that can be analyzed for information on the material the light passed through (O'Connell, 2019).

Figure 2.6 Visual of light being distributed while passing through a prism.
Credit: https://en.wikipedia.org/wiki/The_Dark_Side_of_the_Moon

When analyzing an emission spectrum, most of the spectrum will be dark but a few bright lines will still exist (Bohr's Theory of the Hydrogen Emission Spectrum, 2020). For an absorption spectrum, most of the spectrum will be bright while the energies the atom is able to absorb will be dark (Bohr's Theory of the Hydrogen Emission Spectrum, 2020). The emission and absorption spectra will appear as inverses of each other. To continue the example of hydrogen, the element's emission and absorption spectra can be seen below in Figure 2.7 compared to a continuous spectrum.
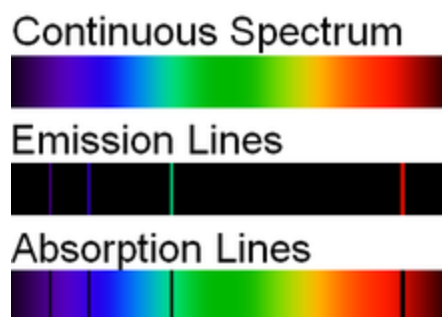
Figure 2.7 Top: Continuous spectrum within the visible light band. Center: Emission spectrum for a hydrogen atom. Bottom: Absorption spectrum for a hydrogen atom. Credit: https://chem.libretexts.org/@go/page/41371

Once scientists know what the emission and absorption spectra of individual elements and molecules look like, they can start looking at more complex systems. This can range from a small volume of gases to an entire galaxy. The same principles apply as they did before but with the addition of how likely it is a photon will hit an atom it can interact with, typically referred to as a radiative transfer model (Ryden, 2010, p. 127). This is calculated by looking at the cross-sectional area of the atom, denoted σ, and the number of atoms within the volume being absorbed, n (Ryden, 2010, p. 128). With these parameters, if the intensity of light being observed before it passes through the object being observed is a known value, I_o, and the depth of the object is given by x, then the intensity of the light on the other side of the observed object will be given by $I(x) = I_o e^{-n\sigma x}$ for each specific frequency of light (Ryden, 2021, p. 129). This will allow for there to be an average intensity of the light spectrum while brighter or darker regions will indicate emission and absorption spectra of individual elements or molecules (Bohr's Theory of the Hydrogen Emission Spectrum, 2020).

Armed with this knowledge, scientists can make sense of emission and absorption spectra from objects larger than a single atom or molecule. They can utilize these spectra to learn what elements are in an unknown gas, the atmosphere of another planet, or even what makes up a star. These spectra are far more complex and require scientists to puzzle out the defining features of different elements or molecular compounds. This puzzling things out is the very nature of spectroscopic science.
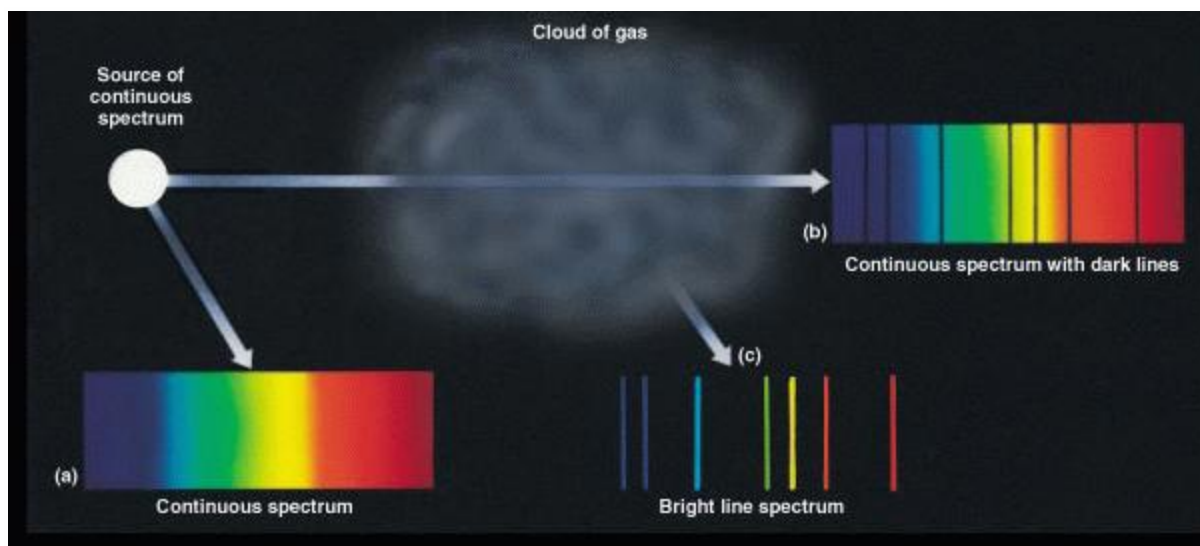
Figure 2.8 Diagram of spectra coming from a cloud of gas. (a) is the continuous spectrum going into the cloud. (b) is the absorption spectrum leaving the cloud. (c) is the emission spectrum leaving the cloud.
Credit :https://faculty.virginia.edu/rwoclass/astr1230/7.2-spectroscopy.html

2.1.4 - Terahertz Spectroscopy

Each way that an atom or molecule interacts with light leads to a different branch of spectroscopy. Atomic spectroscopy and vibrational spectroscopy will not be discussed as they are not relevant to the future content of this project. Instead, we will focus on rotational spectroscopy, specifically as it pertains to terahertz spectroscopy which takes advantage of light in the frequency range of about 0.1-20 THz (Beard, 2002). Terahertz spectroscopy is a somewhat new branch of technology that has helped make great strides in the field of observational astrophysics (Kulesa, 2011). It can be used to analyze the atmospheres of nearby planets or even comments to discern their contents and potentially identify signs of extraterrestrial life. It can help us learn about the interstellar medium and how it has evolved over time, giving us a peek into how stars form and die. It can even help us learn about how stars and galaxies formed in the early universe just after the Big Bang. Each of these ideas will be explored in the results section of this paper.

2.1.5 - Spectral Broadening in Terahertz Spectroscopy

One of the main difficulties in looking at distant objects (especially denser objects like planetary atmospheres) is spectral broadening which refers to when spectral lines get stretched out and become somewhat unclear. There are three categories of this phenomenon; natural broadening, Doppler broadening, and pressure broadening. Natural broadening is created by the Heisenberg uncertainty principle and causes such a small change in the appearance of spectral lines in comparison to Doppler and pressure broadening that it can be effectively ignored in the THz spectral region, at least for the purposes of this project (Science Direct, n.d.). Doppler broadening is created by the relative velocity between the observer and what is being observed. As objects move away from each other wavelengths appear longer and when objects move together wavelengths appear shorter (Young, 2020, p. 524). This aspect of relativity causes emission/absorption lines to become wider (broadened) when molecules in a gas move at different relative velocities to the observer (Science Direct, n.d.). This type of broadening leaves the spectral lines fairly obvious and has a small effect at the longer wavelengths used in terahertz spectroscopy (Science Direct, n.d.) and is used to create velocity profiles of the molecules. Pressure broadening can be a bit more complicated.

Pressure broadening has to do with how interactions between molecules can affect the sharpness of spectral lines starting at about 1×10^{-5} atm (Science Direct, n.d.), as illustrated in Figure 2.9. This isn't a large issue in the interstellar medium where there are not a lot of molecules to bump into each other, but it becomes far more important when looking at denser objects such as planetary atmospheres. As molecules bump into each other they affect the apparent wavelengths of the photons being emitted or absorbed (Science Direct, n.d.). This process has the largest effect on emission/absorption spectra and is the most difficult to overcome, but scientists are still able to account for it using pressure and temperature modeling (Science Direct, n.d.).
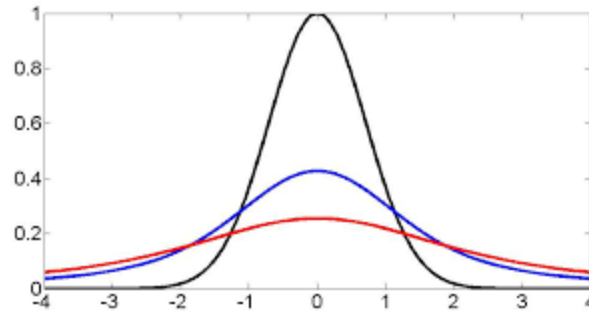
Figure 2.9 Example of a normal spectral line (shown in black) versus a Doppler broadened line (shown in blue) and a pressure broadened line (shown in red). Credit: https://cefrc.princeton.edu/sites/cefrc/files/Files/2013%20Lecture%20Notes/Hanson/pLecture6.pdf

Accounting for spectral broadening when analyzing data is tricky as there is no way to directly eliminate the effect it introduces. The linewidth created by Doppler broadening can be found with the equation $\Delta\lambda = \lambda/c\sqrt{2kT/m}$ where $\Delta\lambda$ is the linewidth, λ is the target frequency, k is the Boltzman constant, T is temperature in Kelvin, and m is the molecular mass (Widths of spectral lines, n.d.). (Science Direct, n.d.). Pressure broadening is a bit more difficult to account for as it requires a known coefficient based on the temperature, pressure, and surrounding gases for each molecule being studied (Science Direct, n.d.). This coefficient needs to be found through experimental and observational work, but once it is found it can be described by the equation $S = \int_{-\infty}^{\infty} k_v \, dv$ where k_v is the pressure dependent absorption coefficient whose spectral width is linearly proportional to pressure (Science Direct, n.d.) and S is the integrated line strength. As shown in Figure 2.9, as the pressure increases, the spectral linewidth gets broader and the peak decreases, preserving the area under the curve, the integrated line strength, making it difficult to identify spectral lines at high pressures.

Section 2.2 - History of ALMA

As mentioned in Chapter 1, the Atacama Large Millimeter/submillimeter Array (ALMA) is one of the most well known observatories for looking at the cosmos in the range of THz, and was first used for observations starting in 2011 following its construction which began in 2004

(ALMA, n.d.). Despite only operating for 10 years now, ALMA has made over 44,000 observations to date, contributing to over 3,000 projects in that time (ALMA Archive, n.d.). At a glance, ALMA is made up of 66 different dishes, with each antenna weighing in at around 100 tons, and can receive signals in a range from 31 GHz - 950 GHz. An initial thought on this might be, "That range does not quite encompass THz, so why is ALMA used to observe stellar objects in a hertz range it cannot receive?" The answer to this has to do with relativistic redshifting, which will be explored in a later section.

The 12-meter dishes can be gently shifted around the desert site into different arrays depending on the object being observed. These shifted arrays can range anywhere from within 150 meters of each other, to a staggering 16 kilometers between the furthest antennas (NRAO, n.d.). The distances in the array setup benefits astronomers in different ways. The spread out arrays let ALMA use a "zoom lens" of sorts to give finer detail in observations, whereas the tightly compacted arrays give a better sensitivity to larger and dimmer stellar objects (NRAO, n.d.).

ALMA has been part of a slew of discoveries since becoming an active radio observation site. The first image ever published by ALMA showed massive concentrations of gas in the collision zones of the Antennae galaxies, which will provide a ripe reserve for future generations of star formation at these zones (ALMA, n.d.). In 2012, while observing a young star similar to our sun, ALMA detected sugar molecules present in the gas surrounding this star. This detection provided evidence to support the claim that the chemical elements required for life to exist might have been present in our solar system during the stage of planetary formation. Since then, ALMA has made findings in areas from spiral structures of mass surrounding stars, protoplanetary discs, all the way to observations of the Juno asteroid (ALMA, n.d.). This report covers another three separate observations made by ALMA and the studies related to those findings. After looking at all of these discoveries and findings, it is clear that ALMA will continue to be at the forefront of astronomical discoveries for years to come, as it has proven to us time and time again its observational prowess.

Section 2.3 - Data Retrieval and Software Used

2.3.1 - How the Data was Retrieved

Data was retrieved from the ALMA archive using the project code given at the end of each study. The data retrieved included raw data, calibrated data, and in some cases the Python scripts that were used. Due to time constraints, we only looked at the calibrated FITS files.

We took the calibrated FITS files and used CARTA to view them. We were able to reach the CARTA viewer one of two ways: through a Jupyter notebook housed on Google Colab, or embedded into the ALMA archive.

2.3.2 - FITS Files

FITS stands for "Flexible Image Transport System" (NASA, n.d.). These files are the most commonly used file type in astronomy. They are usually images, though they can contain much more than that. They can store scientific data sets consisting of multidimensional arrays (in 1D, 2D, or 3D) and 2D tables organized in rows and columns of information. Concerning multidimensional arrays, a 1D array could contain a spectrum, a 2D array could be a table or an image, and 3D arrays could be data cubes. These files are very large in size and cannot be viewed through typical photo-viewing software. This led us to try different softwares before settling on CARTA.

2.3.3 - CARTA

CARTA, also known as the Cube Analysis and Rendering Tool for Astronomy, is a software used for visualizing images from FITS files (CARTA, n.d.). The version available to us from the Jupyter notebook is CARTA v1.1, and the version accessible from the ALMA archive is CARTA v1.4. An example of the CARTA viewer is shown below in Figure 2.10.
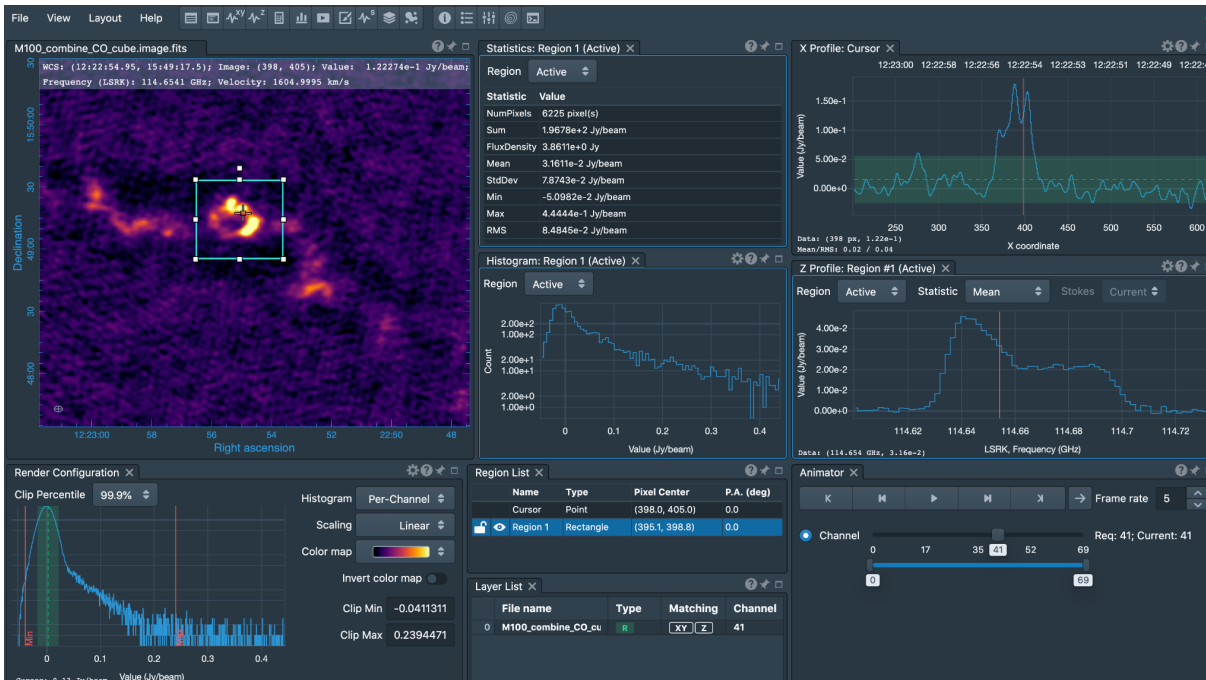
Figure 2.10 Example of CARTA viewer Credit: https://cartavis.org/

CARTA has several widgets that allow the user to view statistics and histograms, as well as the graphs of flux values in the x-, y-, and z-axes. For 3D data cubes, CARTA can animate through the z-axis and lets the user choose which frame they want to look at at a given time. The user can also create regions on the image viewer to look at data values and statistics from only a certain part of the image.

2.3.4 - Google Colab

Google Colaboratory allows for users to write, execute, and share Python code within a browser (Google, n.d.). Notebooks shared in Colab are Jupyter notebooks, and they allow the user to combine executable code, rich text, images, HTML, and more.

Chapter 3: Methods

In order to accomplish the goal of understanding professional techniques for interpreting spectroscopic data collected in the terahertz region for astronomical and observational astrophysical research, this project used the following objectives:

1. Understand applications of terahertz spectroscopy in astrophysical research
2. Identify techniques and technologies used for data processing
3. Learn to process ALMA data using proper techniques and technologies
4. Identify important lessons and questions for further research

Section 3.1 - O III Emission Line in High Red-Shifted Galaxy

The first portion of this project started by looking at how terahertz spectroscopy could be used to analyze regions of star formation in deep space. A study done in 2018, *The Onset of Star Formation 250 Million Years After the Big Bang* (project code 2015.1.00428.S), aimed ALMA into the far reaches of the cosmos to observe the galaxy MACS1149-JD1, or MACS for short, in order to see the potential star formation rate of a high red-shifted galaxy (Hashimoto et al., 2018). This leads us to explore the question, "What is a 'high red-shifted' galaxy?" Put simply, it is a galaxy at the edge of the universe with a redshift value that exceeds all classical redshift-distance calculations, such as Hubble's Law. Hubble's Law states that the distance to a galaxy is proportional to the galaxy's recession velocity as measured by its redshift, $v = H_o\, r$, where v is the recession velocity, H_o is Hubble's constant, and r is the distance (HyperPhysics, n.d.). This formula holds a linear relationship and is good for measuring distances to most galaxies, but this relationship begins to break down after around a redshift value of 1. In order to properly analyze galaxies outside of this range of redshift, a relativistic component needs to be considered in the calculations.
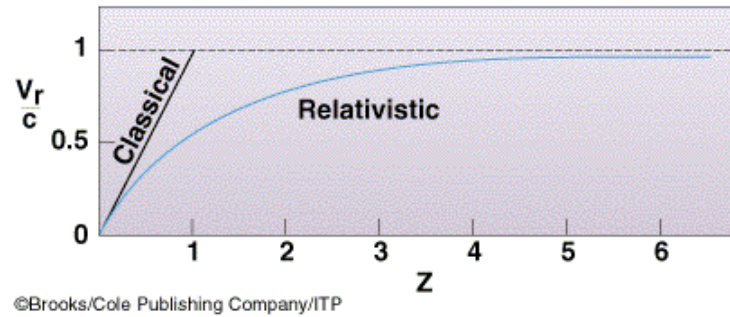
Figure 3.1: A curve representing when the classical versus relativistic redshift
calculations needed to be considered.
Credit: https://sites.ualberta.ca/~pogosyan/teaching/ASTRO_122/lect26/lecture26.html

This relativistic component is found in the calculation of the emitted or observed frequency of wavelengths, used to measure the recession velocity of galaxies, and will be explored in the case of MACS in section 3.1.3. The augmented calculations for classical versus relativistic redshift are important because without them, researchers would be observing or analyzing the wrong part of space, thus leading to results that would vary greatly from the expected.

The study found an emission line of doubly ionized oxygen (O III) at the redshift of 9.1096 ± 0.0006 (Hashimoto, 2018). This is important because concentrations of O III are generally found to be in planetary nebulae and other such star forming regions. Having the redshift determined as accurately as this allowed the observers to draw the conclusion that the optical color (shown below) stems from a stellar component from around 250 million years after the universe's birth, corresponding to a redshift of about 15. Their results proceeded to indicate that similar early episodes of star formation could be detected in other galaxies with future studies with more advanced telescopes (Hashimoto, 2018).
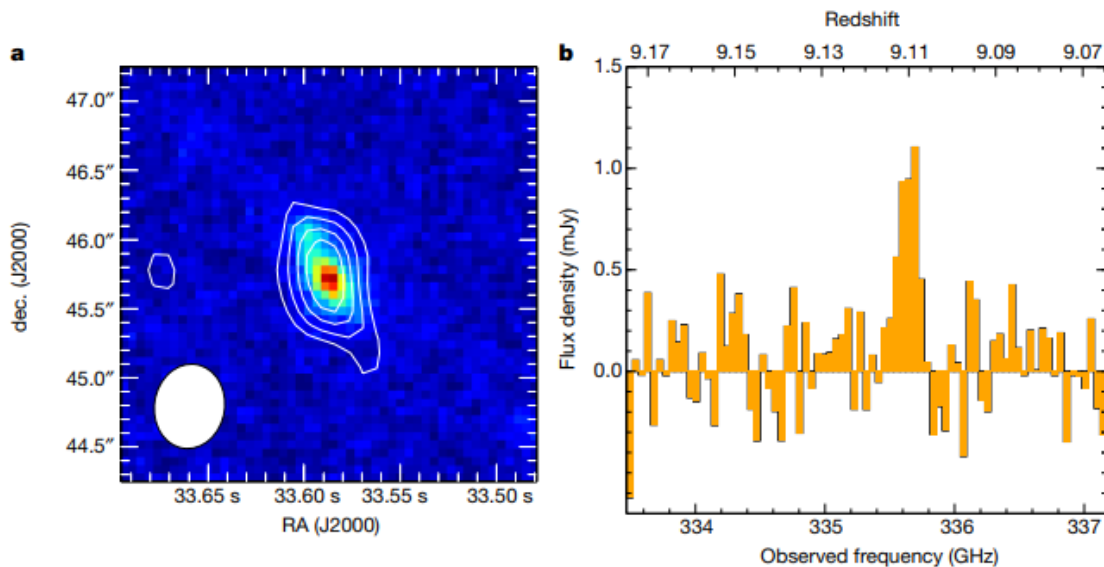
Figure 3.2: HST image image of MACS1149-JD1 with overlaying ALMA [O III] contours (left), and the ALMA [O III] spectrum in frequency space which shows the obtained redshift of 9.1096 (right).
Credit: https://www.nature.com/articles/s41586-018-0117-z#citeas

3.1.1 - What This Tells Us About MACS1149-JD1

Obviously a redshift of 9.1096 and 15 are very different numbers, especially when it comes to galaxies this old. So what exactly is the study trying to tell us about MACS with these different redshift values? The redshift of 15 (15.4 from the study) corresponds to the initial epoch of formation of the galaxy and its first "episode" of star formation, around 250 million years after the Big Bang (Hashimoto, 2018). Due to feedback processes, the star formation rate (SFR) was weakened or even terminated during this time. This held true until gaseous inflow rejuvenated the SFR at the observed redshift of 9.1096, thus leading to the detection of the O III emission lines by ALMA. Although the galaxy is experiencing a second episode of star formation, researchers believe that a majority of the stars present in MACS were birthed in the initial onset of star formation. The results of the study then concluded that it might be possible to detect these earlier episodes of star formation beyond the redshift range currently observable by our present telescopes, such as Hubble (Hashimoto, 2018). In addition, their study also

demonstrated the power that ALMA has to spectroscopically identify galaxies at a redshift of over 9, showing that ALMA will play a pivotal role in studying "first-generation" galaxies.
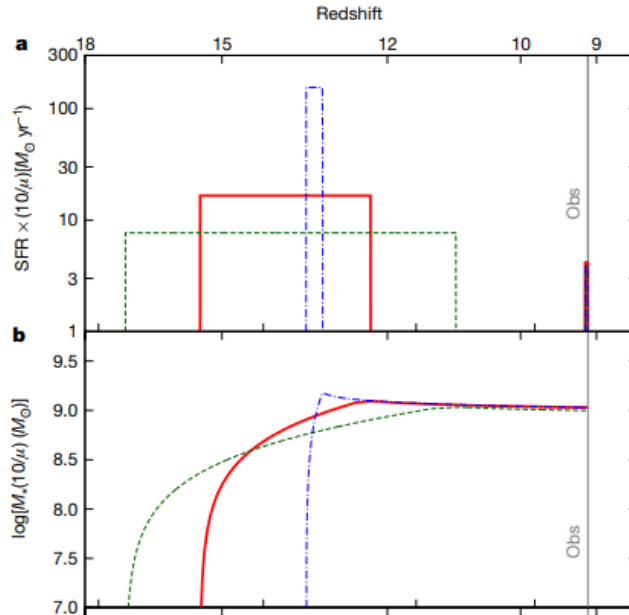
Figure 3.3: Demonstrates the early episode of star formation in MACS as a function of its redshift. Depicts star formation rate (SFR) (top), and stellar mass assembly (bottom). The blue, green, and red lines correspond to star formation bursts of duration 10Myr, 100Myr and 200Myr, respectively. Majority of stellar mass of MACS observed at the gray line (z=9.1096) was produced on an interval of redshift $12 < z < 16$.

3.1.2 - Processing the Data

In order to analyze the data collected from this study, a few different approaches were taken. The first order of business was to extract and download the necessary FITS files from the ALMA data archive. Following this step, there were a few options. The first of which was to use the imaging program CASA run through a Linux terminal window. Our initial understanding of Linux was very limited, so this offered its first round of roadblocks. In order to first use Linux at all, we had to use a virtual machine, Ubuntu, to run Linux on our Windows computers. Though many attempts were made to untar the ALMA files in Linux and pull them into CASA, this option seemed to be a dead end for those with limited computer science experience.

This development led to discovering other methods of analyzing the data images. We were pointed in the direction of using the Google Colab software to use CARTA, as it could be done in a web browser instead of going through the virtual machine. The code we used for pulling up the images is shown below in Appendix A. This proved to be easier and simpler than trying to use Linux, but another obstacle blocked our path, as we could only load a limited amount of files into Google Colab each time we wanted to observe and analyze the images. Our group member Zetta Rajaniemi, along with the advisors for this project, noticed something on the ALMA data request handler page that could help with this problem.

For certain publications of data, this study included, there are shortcuts on the right hand side of the page that take the specific fits files and loads them straight into CARTA, without the need for code to be run through Google Colab.

Figure 3.4: Shows the CARTA shortcuts next to the image files taken from the ALMA
data archive.

Credit: https://almascience.nrao.edu/rh/submission

This simplified the analysis process immensely, and made it much easier to analyze multiple fits files at once, which in turn meant it was easier to compare analysis from file to file, as well as to the original figures from the initial study.

3.1.3 - Image Analysis

After going through the multitude of images from the ALMA archive, the region of interest from the paper was found, shown in Figure 3.5. The square box in the middle of the image acted as a funnel for information, this way unwanted information was not getting thrown in with what we were looking for, or coming from sources that we were not analyzing. The CARTA widget in the bottom middle of the figure shows the observed frequency of 335.6885 GHz.
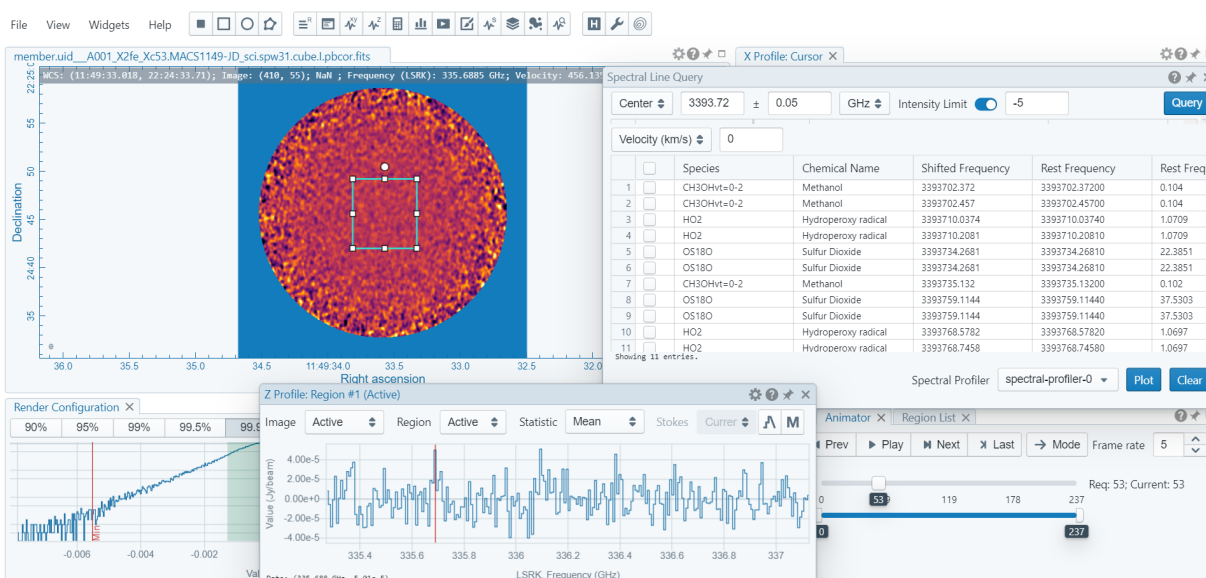
Figure 3.5: A screenshot taken from the CARTA application showing the region of interest (top left), the spectral line query widget (top right), and the observed frequency (bottom middle). Credit:https://carta.almascience.nrao.edu/carta-frontend/?socketUrl=wss://carta.almascience.nrao.edu/fad8aa05d713b3078d6afd33e&file=member.uid___A001_X2fe_Xc53.MACS1149-JD_sci.spw31.cube.I.pbcor.fits

This value for observed frequency, as well as the value for right ascension and declination on the axis of the image, agrees with the values shown in Figure 3.2, so we knew that we were looking in the right region of space. The spectral line widget on the right scans the funneled region of the image for atomic compositions in a certain spectra. This scanning widget is where the relativistic component mentioned earlier comes into play. In order to scan in the right spectra, we have to convert the observed frequency into a relativistic emitted frequency,

which was done with the equation $1 + z = \frac{f_{emit}}{f_{obsv}}$, with z being the observed redshift value taken from the study of 9.1096, causing the observed frequency to be shifted by a factor of about 10. This gave us an emitted frequency of 3.393 THz, right in the realm of terahertz spectroscopic observations. All of this information together heavily suggests that this is the exact region in space and frequency that Hashimoto et al. observed the O III emission lines stemming from MACS.

3.1.4 - Concluding Thoughts and Synthesis

Both the initial study and analysis efforts can be used to showcase ALMA's powerful capabilities of observation. Although, something was noticed about the study piqued our curiosity on the topic of star formation from another source. Earlier in the academic year, one of our authors Jackson Morse assisted in authoring a research paper on relativistic components of black holes. One of the sources that was used for this paper (Adams, 2016) explained the different ages of the universe, with the eventual hypothetical ending of all time. In this source, it was discussed that star formation in the universe did not occur until around 400 million years following the Big Bang. Having this information already in mind, we found it curious that MACS ended up being hypothesized to begin star formation 150 million years earlier than Adams and Laughlin had originally claimed stars and galaxies to begin forming. While the "400 million years" is by no means a hard cutoff for different eras of the universe, it was still intriguing to see two very different numbers throughout different research experiences. This has led to the question, "What if there are more galaxies to discover even older than MACS?" Based on the observations and conclusions of Hashimoto et al., as well as analysis and experience, it is plausible that such galaxies may exist. Though we do not know for certain yet, ALMA as well as the James Webb Space Telescope will help future researchers to answer this question.

Section 3.2 - Dust Production in Supernova 1987A

       The second topic explored in this project looked at data from ALMA concerning supernova (SN) 1987A. SN 1987A is one of the closest observed supernova explosions, which makes it desirable to study supernovae and supernova remnant physics. The data collected in this study (ALMA project code: 2011.0.00273.S) from 2014 was used to determine if supernovae are important sources of dust production (Indebetouw, 2014). This study also used the data to confirm whether or not SN 1987A is a pulsar wind nebula (PWN). Due to time constraints, only the dust production was looked at in detail. The study looked at ALMA receiver bands 3, 6, 7, and 9 (at wavelengths 2.8 mm, 1.4 mm, 870 μm, and 450 μm, respectively).

3.2.1 - Interstellar Dust

       Interstellar dust is comprised of small particles of solid material in space. It is formed in stars, then is blown off in either a slow wind or a massive star explosion (Herschel Space Observatory). These particles are the building blocks for new stars and other celestial bodies. Dust absorbs visible light from surrounding objects and was thus viewed as a nuisance for many years, as it would hide various things from view of telescopes, at least in the visible spectrum. While dust is too cold to radiate in the visible spectrum, it glows in the infrared spectrum and can be detected with telescopes like the *Herschel Space Observatory* (Lumen Learning, n.d.).
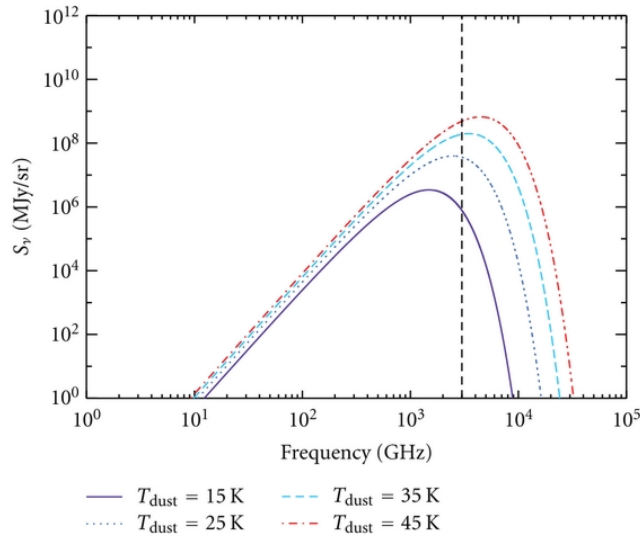
Figure 3.6 Modified blackbody curves for dust emission. Each curve represents the flux density (in megaJanskys per steradian) for a different dust temperature.

Credit: https://www.hindawi.com/journals/aa/2012/124931/

Dust is treated as a quasi-blackbody, and thermal dust emission is represented by blackbody radiation. Figure 3.6 above shows modified blackbody curves for dust emission at different temperatures (Tibbs et al, 2012). We used the Rayleigh-Jeans approximation of Planck's Law, which is used to determine flux densities of blackbody radiation, $B_v(T) = \frac{2v^2 kT}{c^2} \propto T$, where $B_v(T)$ is the flux density, v is the frequency, k is the Boltzmann constant, T is temperature, and c is the speed of light (Walker, 2015). Tibbs et al. found that observations at far-infrared and submillimeter wavelengths showed that the spectrum of thermal dust emission is well represented by the modified blackbody function $S_v \propto \frac{2hv^{3+\beta}}{c^2} \frac{1}{exp(hv/kT_{dust})-1}$, where all variables are the same as the Rayleigh-Jeans approximation except S_v is the flux density and β is the dust emissivity spectral index (Tibbs et al, 2012).

3.2.2 - Why the Study was Conducted

Supernovae have been theorized to be important dust producers for many years with the predictions ranging from 0.1 - 1.0 $M_\odot$ (Indebetouw, 2014). Previous studies of other supernovae

and supernova remnants have not matched this prediction, having measured masses of 10^{-6} - 10^{-3} M$_\odot$ of warm dust (Todini & Ferrara, 2001; Nozawa et al, 2003; Cherchneff & Dwek, 2010). A previous study of SN 1987A from 2011 was the exception, implying 0.4 - 0.7 M$_\odot$ of dust (Matsuura et al, 2011). This study was done with far infrared photometry with the *Herschel Space Observatory*, which caused a discrepancy with previous data. The dust measured could have been both warm and cold dust as *Herschel* did not have sufficient spatial resolution to determine the location of the dust. Data from ALMA in the submillimeter regime is thus desirable to determine where the emission is coming from (Indebetouw, 2014).

3.2.3 What the Study Found

Indebetouw et al. found that the spectrum of the inner ejecta rose steeply with frequency (Indebetouw, 2014). This data does not fit the model of a PWN, though it does fit the model for dust production, as shown below in Figure 3.7.
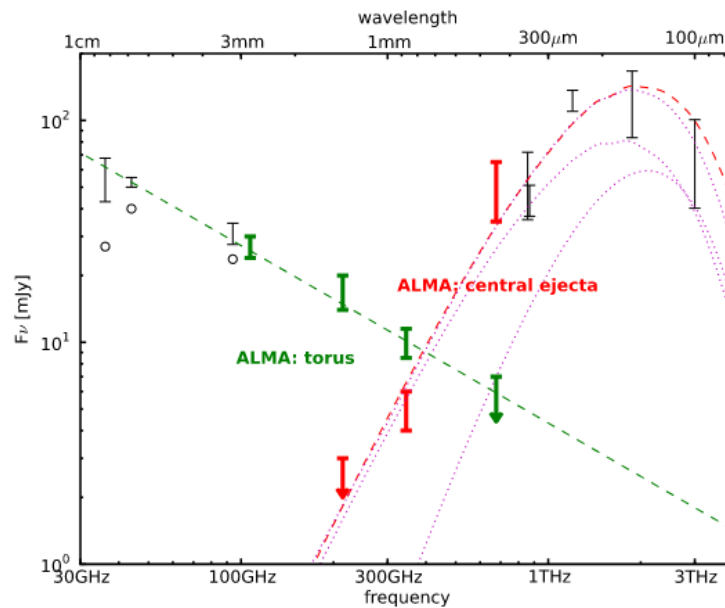
Figure 3.7 ALMA flux densities for the torus (in green) and inner ejecta (in red). The red markers represent the flux densities of the ejecta of bands 6, 7, and 9, with the markers in black representing measurements from previous studies. The flux densities were fit to a model of dust emission (0.23 M$_\odot$ of amorphous carbon dust at 26 K), shown as a red dashed line. The pink dotted line just underneath the red dashed line represents a combination of carbon and silicate dust. Credit: (Indebetouw, 2014)

The data was fit to a model of dust emission representing 0.23 $M_\odot$ of amorphous carbon dust at 26 K (red dashed line above) as well as a combination of carbon and silicate dust (pink dotted line just under the red dashed line). This implies that the carbon dust mass is higher than it was measured in previous studies. The data also implies that nearly all carbon released in the supernova explosion has condensed into dust, for an approximate total mass of 0.23 ± 0.1 $M_\odot$. All of this dust condensed in the cold inner ejecta. Assuming 0.1 $M_\odot$ of it survives the reverse shock to be dispersed into the ISM and that SN 1987A is a typical Type II supernova, the researchers concluded that Type II supernovae could dominate dust production at all redshifts (Indebetouw, 2014).

3.2.4 - Processing the Data

The process of analyzing the data for this study is very similar to what was noted in Section 3.1.2, however this study did not have shortcuts to CARTA on the ALMA data request handler page. For this study, the Google Colab notebook was used to reach CARTA. Something of note is that the CARTA accessed through ALMA is the most updated version, v1.4, and the version accessed through the notebook is v1.1.

This study used a variety of methods in their data analysis that are not possible to recreate through CARTA v1.1. The researchers used different programs to subtract the torus from the inner ejecta for bands 6, 7, and 9 and make different FITS files for both, none of which were available through the ALMA archive (Indebetouw, 2014). They scaled the amplitude, noted below as the flux densities of the inner ejecta gathered in this project were one power of magnitude higher than those in the original study. They also subtracted the torus and ejecta from each other in the Fourier plane, which was also impossible to do in CARTA alone. For this project, only the flux densities for band 3 and the inner ejecta for bands 6, 7, and 9 were collected.

3.2.5 - Data Analysis
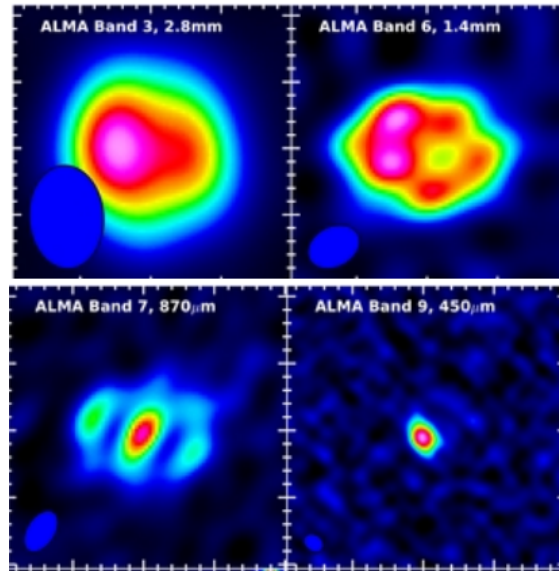
Figure 3.8 Images of SN 1987A at bands 3, 6, 7, and 9 Credit: (Indebetouw, 2014)
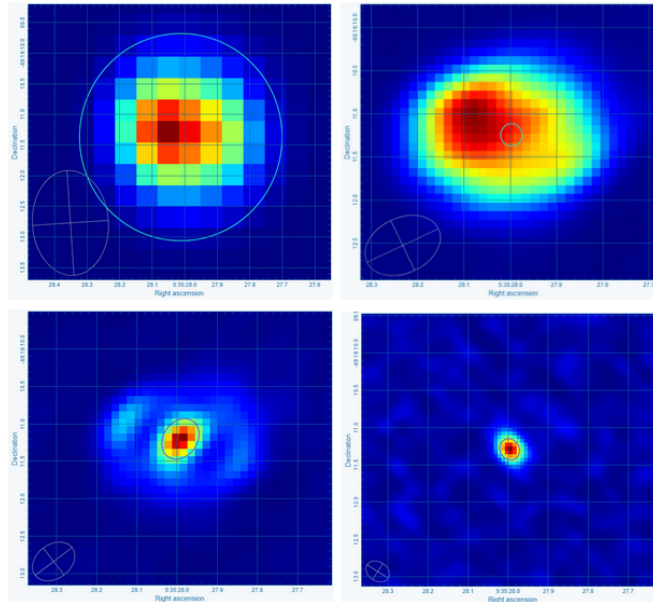
Figure 3.9 Images of SN 1987A at bands 3, 6, 7, and 9 recreated in CARTA. The regions studied are shown in the circles surrounding the ejecta in bands 6, 7, 9, and all of band 3.

Figure 3.8 shows the spatially resolved continuum images of bands 3, 6, 7, and 9 gathered from the original study using ALMA (Indebetouw, 2014). As mentioned in Section 3.2.4, the researchers used various methods in finding the flux values (shown below in Table 1). Figure 3.9 shows the images of bands 3, 6, 7, and 9 recreated from the calibrated FITS files found in the ALMA archive in CARTA. The circles represent the regions studied to find the flux values for the inner ejecta of bands 6, 7, 9, and all of band 3. The statistics widget was used for this part of the project (Figure 3.10). After selecting the region of interest, the "Sum" value over the region represents the flux density of the region, and the "StdDev" value is the standard deviation.
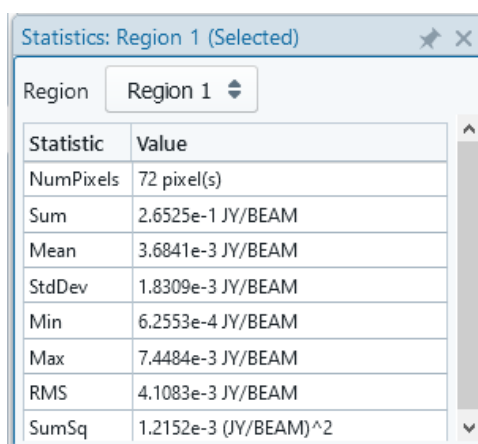
Figure 3.10 Screenshot of CARTA statistics widget for band 3,
where the "Sum" value represents the flux density, and "StdDev" is
the standard deviation.

	Flux density from study (mJy)	Flux density from recreation (mJy)
Band 3 (2.8 mm)	27 ± 3	265 ± 2
Band 6 (1.4 mm)	< 2	14.6 ± 0.1
Band 7 (870 μm)	5 ± 1	50.9 ± 0.4
Band 9 (450 μm)	50 ± 15	533 ± 3

Table 1 Flux densities of bands 3, 6, 7, and 9 (in milliJanksys). The left column has the values from the original study and the right column has the recreated values from CARTA. Credit: (Indebetouw, 2014)

Overall, the flux density values found in CARTA are similar to those found in the original study. They are an order of magnitude higher than the values from the study, as mentioned in Section 3.2.4, though this is likely due to amplitude scaling. They show the same trend, meaning the flux densities of the inner ejecta (bands 6, 7, 9) rise steeply as frequency increases and wavelength shortens (14.6 ± 0.1 mJy, 50.9 ± 0.4 mJy, and 533 ± 3 mJy, respectively). Thus, these values should also fit the model of dust emission pertaining to 0.23 $M_\odot$ of amorphous carbon dust at 26 K (Indebetouw, 2014).

3.2.6 - Conclusions

There is not enough data from this project alone to conclude whether or not supernovae are significant sources of dust production. That would take far more time and more people to prove. However, the data, much in the same way of the original study, does show that SN 1987A fits the model of dust production. Further studies of SN 1987A, or possibly other supernovae, in the submillimeter range could give more evidence, especially as more time passes from SN 1987A's initial explosion. The data also shows how ALMA has strong enough spatial resolution to distinguish between the torus and inner ejecta to determine the location of dust emission.

Section 3.3 - Phosphine in the Cloud Decks of Venus

This final portion of this project began by looking at planetary applications of terahertz spectroscopy. A paper published in late 2020 made the fantastical claim that it had found a potential life sign on Venus with the detection of phosphine in the planet's atmosphere (Greaves, 2020). The discovery had been made using the James Clerk Maxwell Telescope and ALMA, making it a viable candidate for this project. However, only a few months later the study was called into question and the data processing procedures used by the team came under fire and the results were considered controversial (Villanueva, 2020). While exploring a study without such controversy was considered, it was eventually decided that the Venus study could be an excellent learning tool because of the controversy around it. This would allow for a better understanding of how things can go both right and wrong when analyzing terahertz spectroscopy data taken from the ALMA Archive.

3.3.1 - What the Study Found and What Makes it Weird

The original study, published in late 2020, claimed to have found the chemical phosphine in the atmosphere of Venus. The team utilized data taken from ALMA as well as the James Clerk Maxwell Telescope. The observations made by each telescope were taken several years apart and the study showed the same level of phosphine in both datasets of about 20-30 parts per billion (Greaves, 2020). What makes this especially interesting is that phosphine is not typically present in the atmosphere of a Terran planet, such as Venus.

Terran planets typically have oxidized atmospheres, meaning the vast majority of molecules are oxygen-based. Phosphine, however, contains one phosphorus atom and three hydrogen atoms, making it a hydrogen-based molecule. Although some trace amounts of phosphine may show up in a Terran planet's atmosphere after having been delivered by an asteroid or released from the ground, the amount should be virtually undetectable and certainly not stable over several years (Greaves, 2020). Earth is an exception, though. Some microbial lifeforms on Earth produce phosphine, keeping a small supply constantly observable in our atmosphere with a maximum concentration of about 7 parts per trillion (Sousa-Silva, 2020). The idea that a Terran planet should not have phosphine unless it is being readily produced by microbial life led to the idea that if the chemical were found in another Terran planet's atmosphere it would indicate life (Sousa-Silva, 2020).

While it was once imagined that Venus held an almost utopian, Earth-like atmosphere under its thick clouds, scientists learned that was not the case as soon as they began sending probes to the planet. Although Venus may once have hosted life (or at least a survivable atmosphere), a runaway greenhouse effect created an environment that seems incapable of supporting life as we understand it (Ryden, 2010). Venus has an atmosphere of about 95% carbon dioxide, sulfuric acid clouds (and rain), a constant surface temperature of approximately 864°F over the entire planet, and a surface pressure about 100 times greater than that of Earth (Trefil, 2012, p.66-69). With all of these factors, it's no wonder that Venus has come to be known as the place where robots go to die instead of a place where biology goes to live. Still, there is a small chance that life we do not quite understand could exist within the cloud decks of Venus.

The original study claimed that the phosphine may exist in a portion of the Venusian atmosphere known as Hadley Circulation cells (Greaves, 2020). These cells exist at midlatitudes about 50-90km above the surface. This means that this part of Venus's atmosphere has a much lower temperature and pressure than the surface, making it a bit more like Florida than the proper hellscape below (Green, 2020). Although any microbial lifeform living in these cells would still need to be able to handle the carbon-dioxide-rich atmosphere and sulfuric acid clouds, it is conceivable that lifeforms that lived on the surface when Venus was habitable by our standards evolved to live in these cells over time (Greaves, 2020). If the phosphine levels found in the original study are true, then this would seem to be the case. Further research on that subject would tend to disagree, though.

3.3.2 - Contradicting Studies

The first contradiction to the original study came out rather quickly and made a simple case for its unreliability. The observed emission line for phosphine was at 266.945 GHz, which is very close to an emission line for sulfur dioxide at 266.943 GHz (Villanueva, 2020). This contradiction held that the original study could not convincingly discern these two lines. When taking Doppler and pressure broadening into account, it is easy to see how this would be a difficult task. The observed area has a maximum pressure of ~0.5 bar and a temperature of ~350 K (Greaves, 2020; Ando, 2020). The emission line for phosphine would expand to about 472 kHz by Doppler broadening and about 4.23-2.75 GHz by pressure broadening while that of sulfur dioxide would be widened to about 267 kHz by Doppler broadening and about 2.625 GHz by pressure broadening. This much uncertainty in the observations would make it difficult to be certain if the observed emission line was actually at 266.945 GHz or 266.943 GHz (Villanueva, 2020).

Shortly after, another contradictory study was published in *Nature* which made a more thorough claim as to why the original study was incorrect. The original study attempted to remove background noise from their raw data by fitting it to a 12th-order polynomial (Greave, 2020). The study broke down the data into a series of squares with sidelength 1.1 arcseconds that covered the planet's surface (Greaves, 2020). When this process was repeated for the ALMA data, it was found that a false positive was created by allowing any spectral signatures to become

artificially large (Snellen, 2020). An independent analysis that utilized a 3rd-order polynomial instead found that the potential signs of phosphine were statistically insignificant and should not be considered proof of the existence of phosphine within the Venusian atmosphere (Snellen, 2020).

3.3.3 - Processing the Venusian Atmosphere

As the visual similarities between phosphine and sulfur dioxide had already been noted and the processing methods of the original study had already been reanalyzed, this project sought another way to check the validity of the original study. The ALMA data used for the original study can be found in the ALMA ScienceArchive using project code 2018.A.00023.S. This data can be accessed in CARTA using the Google Colab code found in Appendix A or linking to the viewer directly from the ALMA website. Once the data was accessed and the original study fully understood, it was decided to focus on comparing phosphine to deuterated water.

Deuterated water (HDO) is present in the Venusian atmosphere at about 2.5 parts per billion, making it only ⅛ as abundant as phosphine if the original study is correct (Greaves, 2020). Should this hold true, then phosphine should be far easier to spot in the spectroscopic data gathered than HDO. After opening CARTA and selecting the entire planet as a ragion, the spectral viewer was used to test this hypothesis.
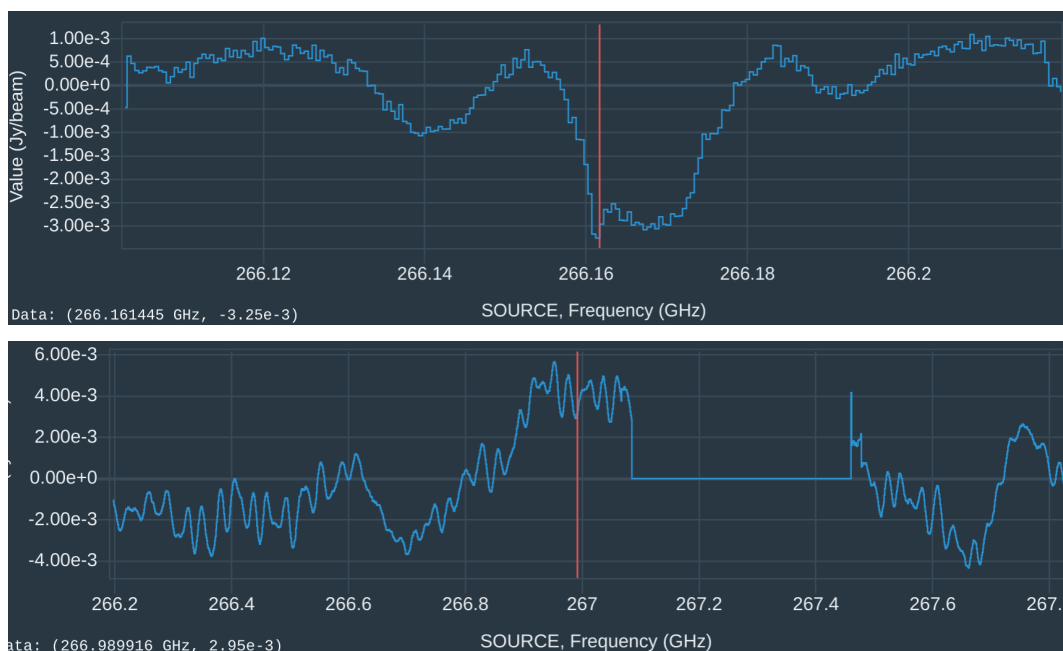
Figure 3.11 The top graph is that of HDO over the surface of Venus as found using the
methods described. The transition frequency of HDO is marked by the red line. The
bottom graph is that of phosphine over the surface of Venus as found using the methods
described. The transition frequency of phosphine is marked by the red line.

Figure 3.11 shows a strong indication of HDO in the top graph with the strong dip
leading to either side of the red line. The rest of the spectrum does not show any similar features.
The bottom graph shows no strong variance around the red line when compared to the entire
spectrum that would indicate the transition frequency of phosphine. The fact that HDO appears
so strongly while phosphine (which should be at least 8 times more abundant) is not noticeable at
all leads to the conclusion that the original paper must have been incorrect about their phosphine
abundance estimates. This coupled with the other criticism and independent reanalysis of the
original study leads this project to the conclusion that there is not, in fact, 20-30 ppb abundance
of phosphine in the atmosphere of Venus.

3.3.3 - Conclusions About Venusian Phosphine

Somewhat unsurprisingly, this project was not able to make a certain determination about
the existence of phosphine within Venus's atmosphere. In order for that question to be
conclusively answered, a probe with uniquely suited spectroscopy tools will need to be sent to

the planet or a containment probe will have to bring some of the planet's atmosphere back to Earth for proper analysis in a laboratory. A proposal for a mission of balloons to be sent to Venus to float through the planet's atmosphere searching for life or other unexpected finds was published in November of 2020 with hopes of launching as early as 2022 or 2023. This portion of the project was still successful, though, as it provided an opportunity to learn about the complexities and difficulties of analyzing ALMA data as well as how to utilize the features of CARTA in concert with other processing tools in order to extract useful information.

Chapter 4: Conclusion

This project was an overall success in learning to understand analysis techniques for astrophysical spectroscopy data in the terahertz region and solve problems that may arise along the way. We were able to identify CARTA as a useful tool for preliminary investigations into astrophysical applications of terahertz spectroscopy. Although CARTA is somewhat limited in its functionality, the applications it does have and the ability to access it directly from the ALMA project archive made it an ideal tool for the students to learn the foundations of astrophysical investigation. It presented us with the opportunity to learn about what scientists do first hand and begin building skills that can be used in future research opportunities.

References

Adams, F.C., & Laughlin, G. (2016). *The five ages of the universe: inside the physics of eternity.* Simon and Schuster.

ALMA. (n.d.). Early Discoveries. Retrieved March 11, 2021, from https://www.almaobservatory.org/en/about-alma-at-first-glance/how-alma-works/early-discoveries/

ALMA Archive. (n.d.). Science Archive. Retrieved September, 2020, from https://almascience.nrao.edu/asax/

Ando, H., Imamura, T., Tellmann, S. *et al.* Thermal structure of the Venusian atmosphere from the sub-cloud region to the mesosphere as observed by radio occultation. *Sci Rep* 10, 3448 (2020). https://doi.org/10.1038/s41598-020-59278-8

Beard, M. C., Turner, G. M., & Schmuttenmaer, C. A. (2002). Terahertz Spectroscopy. *The Journal of Physical Chemistry B, 106*(29), 7146-7159. doi:10.1021/jp020579i

Bellotti, A. (2015). *THE MILLIMETER-WAVELENGTH SULFUR DIOXIDE ABSORPTION SPECTRA MEASURED UNDER SIMULATED VENUS CONDITIONS* (Unpublished master's thesis). Georgia Institute of Technology. Retrieved March 15, 2021, from https://smartech.gatech.edu/bitstream/handle/1853/53444/BELLOTTI-THESIS-2015.pdf

Bohr's Theory of the Hydrogen Emission Spectrum. (2020, September 1). Retrieved March 9, 2021, from https://chem.libretexts.org/@go/page/41371

Cameron, J. M., Bruno, C., Parachalil, D. R., Baker, M. J., Bonnier, F., Butler, H. J., & Byrne, H. J. (2020, May 27). Vibrational spectroscopic analysis and quantification of proteins in human blood plasma and serum. Retrieved March 27, 2021, from https://www.sciencedirect.com/science/article/pii/B9780128186107000104

CARTA. (n.d.). Retrieved May 06, 2021, from https://cartavis.org/

Cherchneff, I., & Dwek, E. (2010, March 16). THE CHEMISTRY OF POPULATION III SUPERNOVA EJECTA. II. THE NUCLEATION OF MOLECULAR CLUSTERS AS A DIAGNOSTIC FOR DUST IN THE EARLY UNIVERSE. *The Astrophysical Journal, 713*(1), 1-24. doi:10.1088/0004-637x/713/1/1

CHIRON. (n.d.). Retrieved March 9, 2021, from http://www.ctio.noao.edu/noao/node/847

Clark, J. (2000). Atomic Orbitals. Retrieved March 11, 2021, from
https://www.chemguide.co.uk/atoms/properties/atomorbs.html

Cosmic Dust. (n.d.). Retrieved May 06, 2021, from
https://courses.lumenlearning.com/astronomy/chapter/cosmic-dust/

Cosmic dust. (n.d.). Retrieved May 06, 2021, from
https://herscheltelescope.org.uk/science/infrared/dust/

DeVorkin, D. H. (2010, July 18). Keck Observatory. Retrieved April 12, 2021, from
https://www.britannica.com/topic/Keck-Observatory

FITS Primer. (n.d.). Retrieved May 06, 2021, from
https://fits.gsfc.nasa.gov/fits_primer.html

Google Colaboratory. (n.d.). Retrieved May 06, 2021, from
https://colab.research.google.com/notebooks/intro.ipynb

Greaves, J.S., Richards, A.M.S., Bains, W. *et al.* Phosphine gas in the cloud decks of Venus. *Nat Astron* (2020). https://doi.org/10.1038/s41550-020-1174-4

Green, H., & Green, J. (Hosts). (2020, September 21). A really old cheetah (No. 258) [Audio podcast episode]. In *Dear Hank & John*. WNYC Studios.

Hanson, R. (2013). Lecture 6: Spectral Lineshapes. Retrieved March 17, 2021, from
https://cefrc.princeton.edu/sites/cefrc/files/Files/2013%20Lecture%20Notes/Hanson/pLecture6.pdf

Hashimoto, T., Laporte, N., Mawatari, K. *et al.* The onset of star formation 250 million years after the Big Bang. *Nature* 557, 392–395 (2018).
https://doi.org/10.1038/s41586-018-0117-z

Hein, A. M., Lingam, M., Eubanks, T. M., Hibberd, A., Fries, D., & Blase, W. P. (2020). A Precursor Balloon Mission for Venusian Astrobiology. *The Astrophysical Journal, 903*(2). doi:10.3847/2041-8213/abc347

Houghton, N. (2020, August 15). Microwave Rotational Spectroscopy. Retrieved March 27, 2021, from
https://chem.libretexts.org/Bookshelves/Physical_and_Theoretical_Chemistry_Textbook_

Maps/Supplemental_Modules_(Physical_and_Theoretical_Chemistry)/Spectroscopy/Rotational_Spectroscopy/Microwave_Rotational_Spectroscopy

HyperPhysics. Retrieved April 19, 2021, from
http://hyperphysics.phy-astr.gsu.edu/hbase/hframe.html

Indebetouw, R., Matsuura, M., Dwek, E., Zanardo, G., Barlow, M. J., Baes, M., . . . Van Loon, J. (2014, January 17). DUST PRODUCTION AND PARTICLE ACCELERATION IN SUPERNOVA 1987A REVEALED WITH ALMA. *The Astrophysical Journal, 782*(1). doi:10.1088/2041-8205/782/1/l2

It's Elemental. (n.d.). Retrieved March 9, 2021, from
https://education.jlab.org/itselemental/ele002.html#:~:text=Helium%2C%20the%20second%20most%20abundant,total%20solar%20eclipse%20in%201868.&text=This%20unknown%20element%20was%20named%20helium%20by%20Lockyer.

Kulesa, C. (2011, September). Terahertz Spectroscopy for Astronomy: From Comets to Cosmology. Retrieved March 27, 2021, from
https://ieeexplore.ieee.org/document/6005336

Matsuura, M., Dwek, E., Meixner, M., Otsuka, M., Babler, B., Barlow, M. J., . . . Sauvage, M. (2011, September 02). Herschel Detects a Massive Dust Reservoir in Supernova 1987A. *Science, 333*(6047), 1258-1261. doi:10.1126/science.1205983

NASA. (2013, March). Electromagnetic Spectrum - Introduction. Retrieved March 11, 2021, from https://imagine.gsfc.nasa.gov/science/toolbox/emspectrum1.html

Nave R. (n.d.). Precession of Spinning Top. Retrieved March 30, 2021, from
http://hyperphysics.phy-astr.gsu.edu/hbase/top.html

Nozawa, T., Kozasa, T., Umeda, H., Maeda, K., & Nomoto, K. (2003, August 11). Dust in the Early Universe: Dust Formation in the Ejecta of Population III Supernovae. *The Astrophysical Journal, 598*(2), 785-803. doi:10.1086/379011

NRAO. (n.d.). Atacama Large Millimeter/submillimeter Array. Retrieved April 15, 2021, from
https://public.nrao.edu/telescopes/alma/

O'Connell, R. W. (2019, May). 7.2 ASTRONOMICAL SPECTROSCOPY. Retrieved March 27, 2021, from https://faculty.virginia.edu/rwoclass/astr1230/7.2-spectroscopy.html

Rotational Spectroscopy of Diatomic Molecules. (2020, August 15). Retrieved March 16, 2021, from https://chem.libretexts.org/@go/page/1840

Ryden, B., & Peterson, B. M. (2010). *Foundations of Astrophysics*. San Francisco, CA: Pearson.

Science Direct. (n.d.). Pressure Broadening. Retrieved March 14, 2021, from https://www.sciencedirect.com/topics/earth-and-planetary-sciences/pressure-broadening#:~:text=Doppler%20broadening%3A%20the%20Doppler%20shifting,source%20of%20the%20radiation%2C%20and&text=pressure%20broadening%3A%20(also%20referred%20to,broadening)%20associated%20with%20molecular%20collisions.

SciShowSpace. (2021, February 05). Maybe There's No Phosphine on Venus | SciShow News. Retrieved March 11, 2021, from https://www.youtube.com/watch?v=XQrhbOugH5Q&t=135s

Siesler, H. W. (2015, November 30). Vibrational Spectroscopy. Retrieved March 27, 2021, from https://www.sciencedirect.com/science/article/pii/B9780128035818013187

Strobel, N (2019, December 17). Telescopes. Retrieved April 12, 2021, from https://www.astronomynotes.com/telescop/s4.htm

Tibbs, C. T., Paladini, R., & Dickinson, C. (2012, December 12). On the Limitations of the Anomalous Microwave Emission Emissivity. *Advances in Astronomy, 2012*, 1-6. doi:10.1155/2012/124931

Todini, P., & Ferrara, A. (2001, August 01). Dust formation in primordial Type II supernovae. *Monthly Notices of the Royal Astronomical Society, 325*(2), 726-736. doi:10.1046/j.1365-8711.2001.04486.x

Trefil, J. (2012). *Space atlas: Mapping the universe and beyond*. Washington, D.C.: National Geographic Partners.

Villanueva, G., Cordiner, M., Irwin, P., De Pater, I., Butler, B., Gurwell, M., . . . Kopparapu, R. (2020, October 28). No phosphine in the atmosphere of Venus. Retrieved from https://arxiv.org/abs/2010.14305

Walker, C. K. (2015). *Terahertz Astronomy*. CRC Press.

Widths of Spectral Lines. (n.d.). Retrieved March 17, 2021, from
     http://www-star.st-and.ac.uk/~kw25/teaching/nebulae/lecture08_linewidths.pdf

Young, H. D., Freedman, R. A., Ford, A. L., & Estrugo, K. Z. (2020). *Sears and Zemanskys
     university physics: With modern physics* (15th ed.). Harlow: Pearson Education Limited.

Appendix A - Google Colab Code Used to Access CARTA for Section 3.3

```python
import os

print("installing pre-requisite packages...")
os.system("apt-get install libgfortran3")

print("installing casatools...")
os.system("pip                      install                   --index-url
https://casa-pip.nrao.edu/repository/pypi-casa-release/simple
casatools==6.1.0.118")
os.system("pip                      install                   --index-url
https://casa-pip.nrao.edu/repository/pypi-casa-release/simple
casatasks==6.1.0.118")

print("downloading   MeasurementSet   from   CASAguide   First   Look   at
Imaging...\n")
os.system("wget
https://almascience.eso.org/dataPortal/member.uid___A001_X13b3_X1f.Venus_s
ci.spw31_51_71.cube.I.manual.pbcor.fits")
os.system("tar -xvf sis14_twhya_calibrated_flagged.ms.tar")

print("make a config file for Google Colab...\n")
os.system("mkdir ~/.casa")
!echo "home      = '/content/'" > ~/.casa/config.py
!echo   "datapath   =   ['`find   /   -type   d   -name   casadata`']"   >>
~/.casa/config.py
!more ~/.casa/config.py


import os
import subprocess as sp
import socket
import signal
import time
import requests
```

```python
FRONT_PORT = '39138'   # make something up
BACK_PORT = '41578'
HOST_IP = socket.gethostbyname(socket.gethostname())

print("downloading ngrok...")
os.system("wget
https://bin.equinox.io/c/4VmDzA7iaHb/ngrok-stable-linux-amd64.zip")
os.system("unzip -o ngrok-stable-linux-amd64.zip");

print("downloading CARTA...")
os.system("wget
https://github.com/CARTAvis/carta/releases/download/v1.4/CARTA-v1.4-RedHat
7.tgz")
os.system("tar -xf CARTA-v1.4-RedHat7.tgz")
os.system("./CARTA.AppImage --appimage-extract")
os.system("rm
squashfs-root/resources/app/carta-backend/lib/libstdc++.so.6")

#cp   =   sp.Popen('CARTA-v1.1-remote/carta   --port='+BACK_PORT   + '
--fport='+FRONT_PORT,  shell=True,  preexec_fn=os.setsid,  stdin=sp.PIPE,
stdout=sp.PIPE, stderr=sp.STDOUT)
cp  =  sp.Popen('./squashfs-root/AppRun  --remote  --port='+BACK_PORT + '
--fport='+FRONT_PORT,  shell=True,  preexec_fn=os.setsid,  stdin=sp.PIPE,
stdout=sp.PIPE, stderr=sp.STDOUT)
gp1  =  sp.Popen('./ngrok  http '  +  HOST_IP+':'+FRONT_PORT,  shell=True,
preexec_fn=os.setsid, stdin=sp.PIPE, stdout=sp.PIPE, stderr=sp.STDOUT)
gp2  =  sp.Popen('./ngrok  http '  +  HOST_IP+':'+BACK_PORT,  shell=True,
preexec_fn=os.setsid, stdin=sp.PIPE, stdout=sp.PIPE, stderr=sp.STDOUT)

time.sleep(2) # give the processes time to start
fcon = requests.get('http://localhost:4040/api/tunnels').json()['tunnels']
bcon = requests.get('http://localhost:4041/api/tunnels').json()['tunnels']
furl  =  [fcon[ii]['public_url']  for  ii  in  range(len(fcon))  if
fcon[ii]['proto'] == 'https'][0]
burl  =  [bcon[ii]['public_url']  for  ii  in  range(len(bcon))  if
bcon[ii]['proto'] == 'https'][0]
print('click    this    ->    '    +    furl    +'/?socketUrl='    +
burl.replace('https','wss'))
```